# Binding Energy and Structure of van der Waals Complexes of Benzene

H. J. Neusser* and H. Krause†

*Institut für Physikalische und Theoretische Chemie, Technische Universität München, Lichtenbergstrasse 4, 85748 Garching, Germany*

*Received January 7, 1994 (Revised Manuscript Received May 25, 1994)*

## Contents



## I. Introduction

The microscopic understanding of intermolecular interaction leading to van der Waals molecules requires the spectroscopic investigation of well-defined finite isolated complexes. A basic physical property to be investigated is the nature and strength of the two-body interaction between the two constituents in a dimer, being the simplest and smallest van der Waals molecule. Among these, dimers of benzene with itself, noble gases, and other molecules are prototype systems for weakly bound van der Waals clusters between nonpolar constituents. Due to the highly symmetric planar structure of the benzene molecule they represent an ideal system for these studies.

In order to elucidate the nature of the van der Waals bonding it is highly desirable to get information about the structure of the van der Waals molecule and on the depth and shape of the van der Waals potential in the dimer. These parameters determine the structure and energetics of larger van der Waals complexes. They are fundamental properties to explain the dynamics in clusters[1] and phase transition between liquid and solid phases.[2,3]

There exists extensive spectroscopic work on benzene-based clusters with vibrational resolution from which structural information was deduced.[4–7] In this review we present data obtained from recent spectroscopic experiments of our group. The main concern of the work is the determination of the energetics of various neutral and ionic dimers of benzene. Two different techniques are used to measure dissociation thresholds of ionic dimers. Besides the breakdown technique observing daughter ion efficiency curves,[8–11] a novel method is presented and described which is based on delayed pulsed field

Hans Jürgen Neusser was born in 1943 in Troppau. He studied physics at the Technical University in Munich where he received his Dr.rer.nat. for work with Professor W. Kaiser. Subsequently he was working with Professor E. W. Schlag and gained his Habilitation in physical chemistry in 1977 for work on the two-photon spectroscopy of molecules in the gas phase. In 1978 he was appointed Privatdozent and 1979 Professor of Physical Chemistry at the Technical University of Munich. In 1983 he received the Chemie–Preis of the Akademie der Wissenschaften zu Göttingen, for his work in the field of two-photon spectroscopy, multiphoton ionization and Doppler-free high-resolution molecular spectroscopy. At present his main interest focus on the laser spectroscopy of molecules and van der Waals complexes, intramolecular dynamics, and the kinetics of ion dissociation.

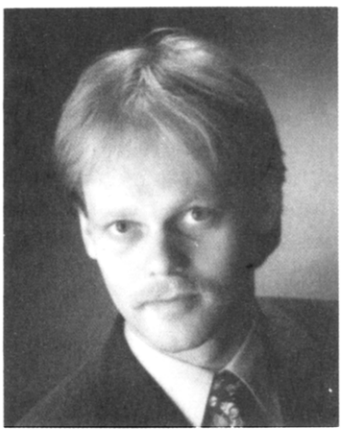

Harald Krause was born in 1962 in München, Bavaria. He studied physics at the Technical University of München, where he received his Diplom in physics in 1988 and the doctoral degree in 1993 from work on state-selected excitation and dissociation of molecular and cluster ions. His research interest concerns the dissociation kinetics and energetics of van der Waals clusters.

† Present address: Institut für Fenstertechnik, Theodor Gietlstrasse 9, 83026 Rosenheim, Germany.

0009-2665/94/0794-1829$14.00/0 © 1994 American Chemical Society

ionization of long-lived Rydberg states close to the ionization energy.[12-14] In this way state-selected benzene–noble gas dimer ions are produced, and we observe their decay in a reflectron mass spectrometer as a function of the selected vibrational state. Pronounced differences in dissociation energy between the neutrals and the ions are found. The strong (10-fold) increase of the dissociation energy in ionic dimers of constituents with delocalized $\pi$ electrons and similar ionization energy points to a strong contribution from charge transfer resonance interaction to the bonding. The dissociation energies of neutral benzene–noble gas dimers obtained with the method of delayed pulsed field threshold ionization are compared with recent theoretical results from other groups. Direct precise information on the structure and the van der Waals bond length of neutral benzene–noble gas complexes arises from their rotationally resolved UV spectra. Structural and energetic results represent basic information on the properties of van der Waals molecules increasing our knowledge about the nature of the van der Waals interaction.

## II. Binding Energies of Molecular Dimers by Breakdown Measurements

### 1. Introductory Remarks

Measurements of breakdown graphs are a well-established technique in the mass spectrometry of molecular compounds. They have produced a variety of data on the energetics of these systems (see e.g. ref 15). The first experiments on hydrocarbons were performed by Chupka and Berkowitz.[16,17] In this work the selectivity of the resonance-enhanced two-photon ionization is combined with the observation of the metastable decay of small homo- and hetero-van der Waals clusters of polyatomic molecules. In our technique the breakdown of the daughter ion intensity with decreasing two-photon energy is recorded to obtain the dissociation threshold of specific decay channels. It will be shown that a wealth of information on the dissociation energy of neutral and ionic dimers and even larger complexes is obtained with this technique.

In a dissociation reaction without reverse activation energy simple relations between the dissociation energy $D_0$ of the neutral dimer $X_2$, the dissociation energy $E_0$ of the ionic dimer $X_2^+$, and the ionization energies of the monomer X and the dimer $X_2$ exist:

$$D_0(X_2) = AE - IE(X) \quad (1)$$

$$E_0(X_2^+) = AE - IE(X_2) \quad (2)$$

Here IE(X) and IE($X_2$) are the ionization energies of the monomer and the dimer, respectively. AE is the appearance energy for the dissociation of the dimer ion $X_2^+$ into $X^+$ and X. By using these relations the dissociation energies of the neutral and the ionic dimer can be determined from the measured ionization energies of the monomer and dimer and the appearance energy. Equations 1 and 2 can be easily extended to heterodimers and larger complexes.

The main problem with the determination of the dissociation energy is a kinetic shift of the appearance energy from this threshold. Generally, it can be expected to be smaller when a slow decay of the ion is monitored. Particularly for benzene dimers with a relatively small dissociation energy below 1 eV we have shown that the restricted phase space of the van der Waals modes[18] leads to negligible kinetic shifts.[9]

A general problem in a cluster experiment with supersonic cold molecular beams is the variety of complexes of different sizes and the monomers that are produced simultaneously. It is difficult to distinguish between monomer ions that have been produced by ionization of a neutral monomer and monomer ions originating from the rapid dissociation of the dimer ion. The situation is clear when a metastable decay channel is observed since monomer ions produced in this way can be well separated from the monomer ions produced by direct ionization of the neutral monomers, e.g. in a reflection mass spectrometer operated in the partial correction mode[8,19] (see below).

Moreover, the selectivity of resonance-enhanced two-photon ionization allows one to selectively ionize, e.g. the dimer, and to suppress the signal from a direct ionization of the monomer. A necessary precondition for this is that the intermediate states of both species are sharp and well separated from each other, this being the case for a variety of molecules and dimers.

Another crucial point for the application of the relations in eqs 1 and 2 is the ionization energy. Strictly speaking, the adiabatic ionization energy has to be known to find exact dissociation energies rather than lower limits. This is no problem for the monomers since here the ionization thresholds are sharp and can be found with an accuracy of a few reciprocal centimeters. However, it turns out to be a problem for dimers, particularly if geometrical changes from the neutral to the ionic dimer occur (e.g. from a T-shaped to a sandwich structure).[20] Here vertical transitions to higher vibrational states in the intermolecular potential are the strongest ones, and the adiabatic transition is weak and its position cannot be identified. As a general rule we may assume that a very sensitive measurement of the ion current leads to ionization energies close to the adiabatic ionization energy.

In order to confirm this, we recorded photoionization efficiency curves of complexes following their two-color two-photon ionization using different intermediate states. In principal one expects that the Franck–Condon factors for transitions to the electronic ground state of the cluster ion should change for different intermolecular modes of the cluster in the intermediate state. Additionally, it should be mentioned that autoionization resonances, as observed for several van der Waals dimers,[21-23] could strongly enhance the transition probability to the ionic ground state. On the other hand, in some clusters with small geometrical changes during the ionization process, sharp onsets of the ionization are observed.[1-,24] Here the technique of pulsed field ionization which will be described below in section III.2 can be applied to find very accurate values of the adiabatic ionization energy.

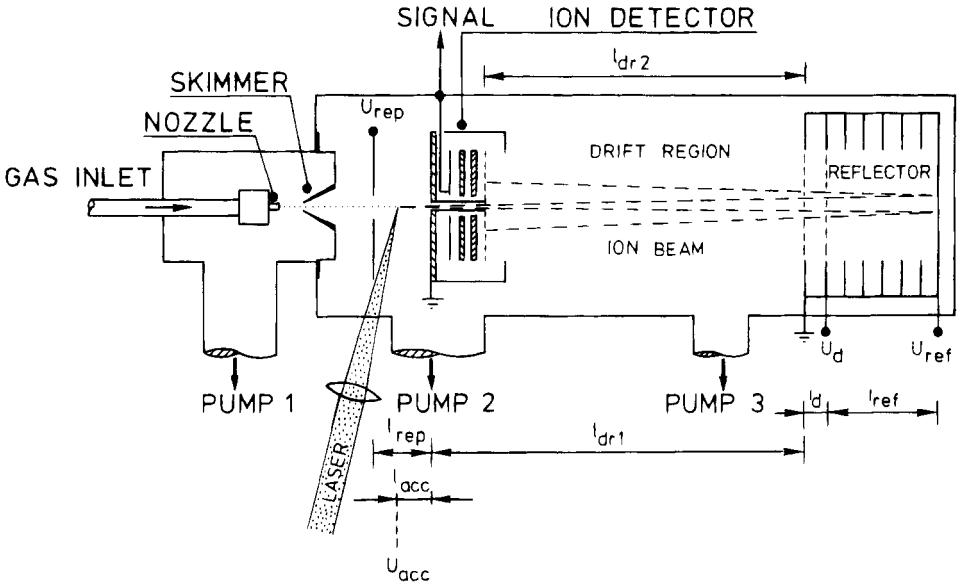


**Figure 1.** Schematic drawing of the linear reflectron mass spectrometer that has been used for the experiments described in this work. The molecular beam produced by a pulsed nozzle is skimmed and collinear to the ion flight paths. The ions are produced by multiphoton ionization in one or two laser beams of different color. After acceleration they pass a small hole in the channel plates and are reflected by 180° in the reflecting field toward the channel plates.

## 2. Experimental

The details of the experimental setup were described in our previous work.[9] A scheme of the set up is shown in Figure 1. Benzene homoclusters or heterogeneous van der Waals clusters of benzene (B), *p*-difluorobenzene (F), toluene (T), and cyclohexane (C) are produced in a supersonic jet expansion of a gas mixture, consisting of 20 mbar of each monomer component seeded in noble gas (He) at a pressure of 1−5 bar. The gas mixture is expanded through a pulsed 200 $\mu$m diameter nozzle orifice and the central part of the beam is selected by a skimmer before it enters the mass spectrometer in a collinear configuration.

The clusters are ionized by resonance-enhanced two-color two-photon ionization in the acceleration region of a linear reflectron time-of-flight (RETOF) mass spectrometer.[9] In the linear RETOF the metastable ion intensity for the different decay channels of a heterocluster ion can be measured with high precision for different decay channels and clusters since the ion trajectories are independent of the kinetic energy of the observed ions. This is different from the situation in a reflection with an angle leading to energy-dependent ion paths.[9]

In order to determine the ionization energy (IE) of the clusters, photoionization efficiency curves were recorded by observation of the ion signal of the respective cluster for a fixed photon energy of the first laser, tuned to the resonant intermediate state but a varying photon energy of the second laser. To find the appearance energy of a dissociation channel, we recorded the intensity of daughter ions that are produced by slow, metastable dissociation of the parent cluster ion in the field-free drift region of the RETOF instrument. The onset of the metastable signal yields the appearance energy (AE) of the observed dissociation channel.

For the investigation of the appearance energy (AE) of a selected decay channel of a cluster ion, the linear RETOF is operating in the partial correcting mode.[19] This technique was described in our previous work.[8,19] Briefly, a metastable decay in the drift region of a TOF mass spectrometer causes a difference in kinetic energy of the parent and daughter ions according to eq 3.

$$\Delta E = E_{kin}(1 - m/M) \tag{3}$$

Here $E_{kin}$ is the kinetic energy of the parent cluster ions and $M$ ($m$) is the mass of the parent (daughter) ions. By operating the reflectron mass spectrometer in the partial correcting mode,[19] the metastable drift signal appears between the peaks of the stable ions of masses $M$ and $m$. This means the reflector is acting as an energy analyzer. In this mode daughter ions produced by a cluster decay in the field-free drift region of the RETOF can be observed as separated peaks (drift peaks). This is shown in Figure 2 for the dissociation of the $B_2^+$ dimer ion into a $B^+$ ion and a neutral B molecule. In this experiment a delay of 20 ns between the first and the second laser pulse was chosen. Therefore the ion signal originating from two-color two-photon ionization is well separated from the signal produced by one-color two-photon ionization of the first laser alone. Both drift peaks due to one- and two-color ionization are marked by arrows in the upper mass spectrum showing the drift peaks on an enlarged scale. Similar mass spectra were recorded for all investigated homo- and heterodimers. The expansion conditions were chosen such that the intensity of larger clusters, e.g. the trimer ion, is 1000 times smaller compared to the dimer intensity. Thus dissociation from larger clusters into the dimer ion can be neglected. The laser power is chosen so that photoionization of the dimer is maximized and, at the same time, the ion yield for smaller masses, resulting from fragmentation after three-photon absorption, is minimized.

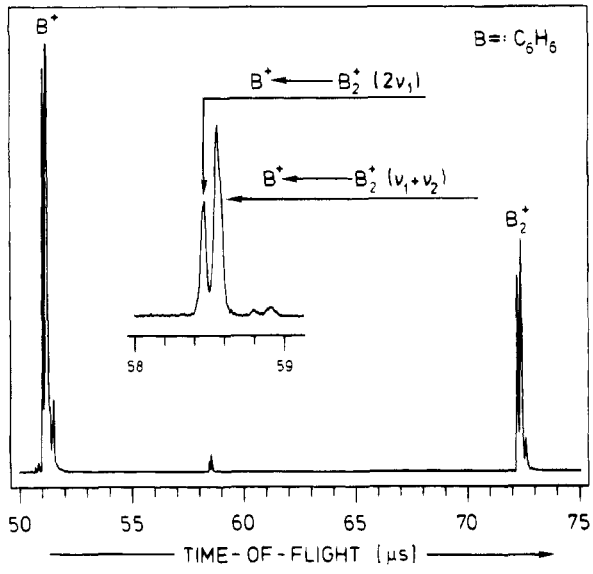


**Figure 2.** Part of the time-of-flight mass spectrum of the benzene dimer ($B_2$) when operating the reflectron in the partial correction mode. The small peaks at 58.5 $\mu$s (see inset) are due to a metastable decay of the benzene dimer cation ($B_2^+$) in the drift region of the reflectron mass spectrometer depicted in Figure 1. Ionization was achieved in a two-laser, two-color experiment with the second laser pulse delayed by 100 ns. The first mass peak originates from an excitation of two photons with $h\nu_1$, while the second stronger peak is a two-color signal due to the absorption of one photon from each laser beam ($h\nu_1 + h\nu_2$).

## 3. Results

The technique described above has been applied to a variety of homo- and heterodimers. A typical result for the breakdown of the metastable intensity is shown in Figure 3 for the benzene ($B_2$) and toluene ($T_2$) homodimer and the benzene–toluene heterodimer (BT).[9] The appearance energy is determined with an accuracy of about 10 meV. Figure 4 displays the onset of the ion current of $B_2$ near the threshold. The arrows indicate the smallest photon energy leading to an ion current above the noise level. The lower trace shows the ion current after excitation of the $6^1$, $S_1$ vibronic state with the first photon. In order to vary the Franck–Condon factors for the transition from the intermediate to the ionic ground state in the upper spectrum an intermediate state including the excitation of an intermolecular vibration[25] was used. The identity of this state is not clear. For this reason we have also chosen other van der Waals intermediate states, but obtained basically the same result as shown in Figure 4. Here, both intermediate states yield the same ionization threshold within the error limits of the experiment. Because of this result and the high sensitivity of our experiment we believe that this value is close to the adiabatic IE.

All results for the IE's and AE's are listed in Table 1 together with the deduced dissociation energies $D_0$ and $E_0$ of the neutral and ionic dimers, respectively. We would like to mention that for the determination of the neutral dimer dissociation energy $D_0$ the very accurate IE's of the monomer are used (see eq 1). Thus an error due to an uncertainty of the IE can be excluded in this case. It is interesting to discuss the results in a systematic way in terms of the different

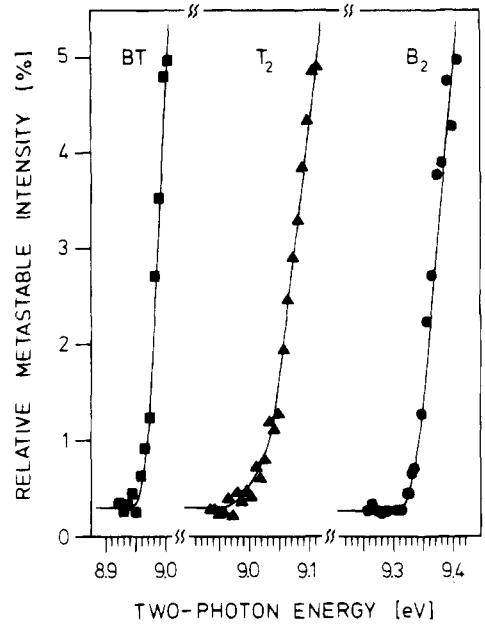


**Figure 3.** Breakdown of the intensity of the metastable ion peaks for three dimers, benzene–toluene (BT), toluene–toluene ($T_2$), and benzene–benzene ($B_2$). The relative intensities are plotted as a function of the two-photon excitation energy. The appearance energy of the metastable decay is taken as the intercept of the breakdown graph with the constant noise level baseline produced by three-photon absorption.

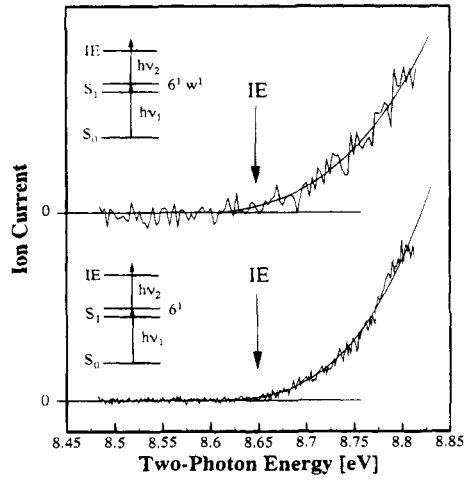


**Figure 4.** Ionization efficiency curves as a function of the two-photon energy $h\nu_1 + h\nu_2$ for two different intermediate states of the resonance enhanced two-photon ionization process: (bottom) the $\nu_6$ intramolecular mode is excited in the $S_1$ intermediate state; (top) in addition to the $\nu_6$ mode an unassigned intermolecular (van der Waals mode) is excited. In both cases the same ionization energy (IE) is obtained. For interpretation, see text.

properties, e.g. polarizability, dipole moment, etc., of the molecules. Since benzene ($\alpha$ = 10.6 Å$^3$ [26]) and *p*-difluorobenzene ($\alpha$ = 10.3 Å$^3$ [26]) have no dipole moment and nearly the same polarizability, the dissociation energies $D_0$ of $B_2$, $F_2$, and BF are expected to be nearly the same. This is in full agreement with our experimental data. Toluene has a small dipole moment ($\mu$ = 0.38 D[27]) and a slightly larger polarizability ($\alpha$ = 12.6 Å$^3$ [26]) compared with those of benzene and *p*-difluorobenzene. This agrees with the experimental finding that $D_0$ is larger for the BT and $T_2$ dimer.

**Table 1. Measured Ionization Energies (IE) and Appearance Energies (AE) of the Metastable Dissociation Channels Discussed in the Text, and Dissociation Energies $D_0$ and $E_0$ of the Neutral and Charged Clusters, Respectively[a]**

| neutral Dimer | ionization energy, (IE), eV | dissociation energy ($D_0$), meV | main intermolecular interactions | dimer cation | appearance energy (AE), eV | dissociation energy ($E_0$), meV | main intermolecular interactions |
|---|---|---|---|---|---|---|---|
| benzene–benzene | 8.65 ± 0.01 | 70 ± 10 | dispersion | (benzene–benzene)$^+$ | 9.31 ± 0.01 | 660 ± 20 | CTR |
| benzene–cyclohexane | 9.12 ± 0.02 | 80 ± 20 | dispersion | (benzene–cyclohexane)$^+$ | 9.32 ± 0.02 | 200 ± 40 | electrostatic |
| toluene–toluene | 8.34 ± 0.01 | 150 ± 10 | dispersion dipole-dipole | (toluene–toluene)$^+$ | 8.97 ± 0.01 | 630 ± 20 | CTR |
| benzene–toluene | 8.42 ± 0.01 | 130 ± 10 | dispersion dipole-ind. dipole | (benzene–toluene)$^+$ | 8.95 ± 0.01 | 530 ± 20 | CTR |
| *p*-DFB–*p*-DFB | 8.87 ± 20 | 90 ± 20 | dispersion | (*p*-DFB–*p*-DFB)$^+$ | 9.25 ± 0.02 | 380 ± 40 | CTR/electro-static |
| benzene–*p*-DFB | 8.75 ± 0.02 | 80 ± 20 | dispersion | (benzene–*p*-DFB)$^+$ | 9.24 ± 0.02 | 490 ± 40 | CTR |

[a] The errors represent the reproducibility of the measured values. CTR, charge-transfer resonance interaction; *p*-DFB, *p*-difluorobenzene.

Several theoretical methods have been applied to calculate the binding energy of the benzene dimer. van de Waal[28] assumed a nearly parallel arrangement of the two benzene molecules and calculated a binding energy of 114 meV, employing potential-energy minimization with empirical atom–atom potential functions. Similar results were obtained by de Meijere and Huisken.[29] This structure, however, is at variance with the T-structure in the benzene crystal. In ab initio calculations, a T-structure was found as the most stable structure of the benzene dimer. In an early work of Čársky et al.[30] a binding energy of 65 meV was calculated and in a more recent study by Hobza et al. a higher binding energy of 117 meV was obtained.[31] When comparing the theoretical results with the experimental values presented here, it must be recognized that the calculated binding energies yield the energy of the potential minimum $D_e$, whereas the experimental ones represent the lowest vibrational energy level $D_0$ (see for example Figure 4 in our previous work[9]). The results differ by the zero-point energy of the multidimensional van der Waals potential.

For ionized van der Waals clusters, electrostatic and charge-transfer resonance interactions (CTR) are strongly enhanced, leading to an increased dissociation energy compared to that of the neutral dimers. For example, for the benzene dimer the binding energy increases by nearly 1 order of magnitude from 70 to 660 meV when the dimer is ionized. Thus ionization goes along with a strong structural rearrangement of the complex. While the neutral benzene dimer is supposed to have a T-shaped structure the dimer cation stabilized by charge transfer resonance interaction should have a sandwich structure with a parallel arrangement of the two benzene planes. Charge-transfer resonance interaction is known to stabilize charged dimers of aromatic molecules.[32] In early theoretical work, McConnell studied charge transfer in negative aromatic radical ions between two phenyl groups linked by a polymethylene chain.[33] For heteroclusters the strength of this interaction decreases when the differences in the ionization energies of the monomers increases. A large difference in the ionization energies leads to a localization of the charge at the component with the lower ionization energy and thus to a small charge transfer-resonance interaction. Therefore bonding of the homodimers is expected to be stronger than that of the heterodimers. From Table 1 it can be seen that indeed the dissociation energies $E_0(B_2^+)$ and $E_0(T_2^+)$ are nearly the same and significantly higher than $E_0$-$(BT^+)$. In the case of $F_2^+$ the lowering of the dissociation energy is attributed to a partial charge localization at the electronegative fluorine atom, which most probably leads to a decreased charge-transfer resonance interaction.

It is interesting to study the contribution of the charge-transfer resonance interaction to the bonding in van der Waals dimer ions in more detail. For this reason we investigated the extreme situation of an heterodimer consisting of an (aromatic) benzene and the nonaromatic cyclohexane molecule. Following two-photon ionization, benzene–cyclohexane dimer ions ($BC^+$) show a slow metastable dissociation in the drift region of the RETOF leading to benzene daughter ions ($B^+$) and neutral cyclohexane molecules (C). The first laser frequency was fixed to the $6_0^1$ transition in benzene and the energy of the second photon was changed. The appearance energy of the above-mentioned decay was found to be 9.32 eV and the ionization energy 9.12 eV. With the use of these values the binding energy of the neutral dimer and the dimer ion are calculated from eqs 1 and 2, respectively, to $D_0(BC) = 80$ meV and $E_0(BC) = 200$ meV (see Table 1). The binding energy in the neutral heterodimer $D_0(BC) = 80$ meV is equal or nearly the same as in $B_2$, BF, and $F_2$ dimers. Since all of these molecules (B, F, C) have no dipole moment and their polarizabilities do not differ very much (cyclohexane $\alpha = 10.9$ Å$^3$ [26]), this result is in line with simple theoretical arguments. The binding energy in the heterodimer ion ($BC^+$) is $E_0(BC^+) = 200$ meV. If we suppose that no charge-transfer resonance interaction contributes to the bonding in $BC^+$ (because of a missing delocalized $\pi$-electron system in cyclohexane) the bonding in $BC^+$ is purely electrostatic. By comparing the data of the benzene dimer $B_2^+$ *with* charge-transfer resonance interaction ($E_0 = 660$ meV) and $BC^+$ *without* charge-transfer resonance interaction ($E_0 = 200$ meV), we conclude that the contribution of charge-transfer resonance to the binding energies is up to 400 meV in sandwich-like dimers of aromatic components.

Experimental values from literature for the binding energy of dimer ions have been obtained from high-pressure mass spectrometry (HPMS) experiments.[34,35]

The most recent value of Mautner (Meot-Ner) et al. is $E_0(B_2^+) = 740 \pm 65$ meV.[34] This is in reasonable agreement with our result. New results of Hiraoka et al.[35] point to a somewhat higher binding energy for the dimer of $E_0(B_2^+) = 894 \pm 43$ meV.

## III. Structure and Binding Energies of Benzene–Rare Gas Complexes

Benzene–rare gas complexes are the simplest complexes with an aromatic molecule as one constituent. The other constituent, a rare gas atom, has an isotropic polarizability and no vibrational internal degree of freedom. Thus the complex molecule has only three additional vibrations compared to the 30 normal vibrations of benzene. These additional vibrations can be well separated from the benzene intramolecular vibrations since their frequency is much lower due to the weak van der Waals interaction. This is different from hydrogen-bonded complexes where the stronger hydrogen bonding leads to higher intermolecular vibrational frequencies and a stronger perturbation of the intramolecular frequencies. Particularly, for the $C_6H_6$·X (X = Ne, Ar, Kr, Xe) dimers we observe a weak perturbation of the benzene vibronic spectrum after attachment of the rare gas atom. Furthermore, due to the high symmetry of the benzene molecule a highly symmetric structure of the benzene–rare gas dimer is expected which facilitates the structure determination on the basis of rotational spectroscopy as described in the first part of this section. Benzene–rare gas complexes do not undergo strong structural changes during the ionization process. This allows one to apply the newly developed technique of delayed pulsed field threshold ionization for vibrationally resolved ion spectroscopy. The results will be discussed in the second part of this section.

### 1. High-Resolution UV Spectroscopy

#### 1.1. Experimental

The goal of high-resolution spectroscopy is to resolve individual transitions rather than to observe broad bands consisting of many overlapping lines. The latter is the normal situation in the conventional Doppler-limited UV spectroscopy of polyatomic molecules. In this work a skimmed supersonic molecular beam is used to reduce the transverse velocity distribution and consequently the Doppler width. Therefore conventional one-photon absorption yields rotationally resolved spectra if narrow bandwidth lasers are used.[36]

In a supersonic beam it is impossible to selectively produce a single cluster species but rather in addition to the monomer a variety of clusters is produced. The spectra of these species may overlap and often an assignment of fluorescence excitation spectra is difficult or even impossible. A powerful method to measure spectra of selected species in a mixture is resonance-enhanced two-photon ionization combined with mass-selective detection.[37] The advantage of resonant two-photon ionization is that the created ions can be registered separately according to their mass in a mass spectrometer. This property of resonance-enhanced two-photon ionization was recognized at an early date[38] and is quite essential to the spectroscopy of van der Waals complexes.[39–41] Namely, a mixture of complexes of different composition and size whose spectra often overlap is produced in a cooled supersonic beam. A mass-selective recording of the spectra facilitates the measurement of a spectrum without interference with spectra of other complexes present in the molecular beam.

Recently, we have shown that a resolution of 120 MHz in a resonance-enhanced two-photon ionization experiment with mass-selective detection can be realized.[42] This resolution is possible in a two-laser experiment consisting of a pulsed amplified cw laser with a bandwidth of 70 MHz. The scheme of the experimental set up is shown in Figure 5. Here, $C_6H_6$·Ar clusters are produced in a supersonic molecular beam. The central part of the molecular jet is selected by a skimmer and enters a second vacuum chamber evacuated by a second turbomolecular pump. Downstream (7.5 cm) of the skimmer aperture benzene molecules and/or clusters interact with the frequency-doubled light of a pulsed amplified cw single-mode dye laser.[43] The frequency width of the pulsed UV light is close to the Fourier transformation of the pulse length and the geometry of the molecular beam–light interaction region has been chosen such that the Doppler width is reduced to about 40 MHz.[44] The laser beam is not focused and the pulse energy is kept as low as 1 $\mu$J in order to avoid saturation of the observed one-photon transitions and further absorption to the ionization continuum. In two-color experiments the second absorption step to the ionization continuum is induced with a delay of 7 ns by the frequency-doubled light of a dye laser which is pumped by the second beam of the excimer laser and operates at a fixed wavelength of 547.7 nm and a frequency width of 0.4 $cm^{-1}$.

The ions produced by the two-photon absorption process are mass selected and detected in a simple home-built time-of-flight mass spectrometer with a field-free drift length of 20 cm and a resulting mass resolution of $m/\Delta m \approx 200$. The mass resolution is sufficient to separate the various species that are present in the molecular beam, e.g. the monomer $C_6H_6$ (78 u), $C_6H_6$·Ar (118 u), and $(C_6H_6)_2$ (156 u) from each other.

#### 1.2. Rotationally Resolved Spectra of Benzene–Noble Gas Dimers

First we discuss the simplest complexes consisting of a single noble gas atom attached to the benzene surface. For illustration of the enormous increase of spectral resolution in Doppler-free spectroscopy in Figure 6 the spectrum of the $6_0^1$ band of $C_6H_6$·Ar is shown for two different resolutions.[45] The $6_0^1$ band is the strongest band in the $S_1 \leftarrow S_0$ spectrum of benzene. It represents a false origin since the pure electronic $S_1 \leftarrow S_0$ transition is forbidden by symmetry and parity and induced by Herzberg–Teller coupling through the $\nu_6$ vibrational mode. As mentioned above, the vibrational structure of the $S_1 \leftarrow S_0$ transitions is only slightly perturbed by the weakly bound Ar atom. Accordingly, the $6_0^1$ band is shifted

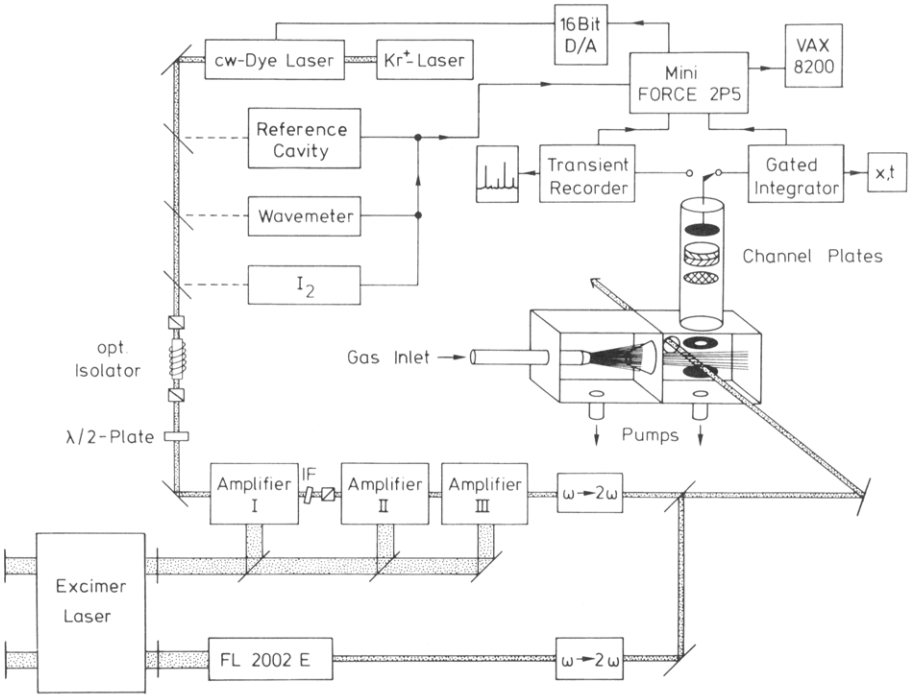


**Figure 5.** Experimental setup for the recording of rotationally resolved UV spectra of van der Waals complexes by mass-selected resonance-enhanced two-photon ionization. A high spectral resolution of the excitation laser of 120 MHz is obtained by pulsed amplification of a single-mode cw dye laser and subsequent frequency doubling. The excited molecules are ionized by the UV light generated in a second dye laser. To select spectral features of a particular cluster molecule, the different ions produced are mass analyzed in a simple time-of-flight mass spectrometer with channel plates as ion detector.

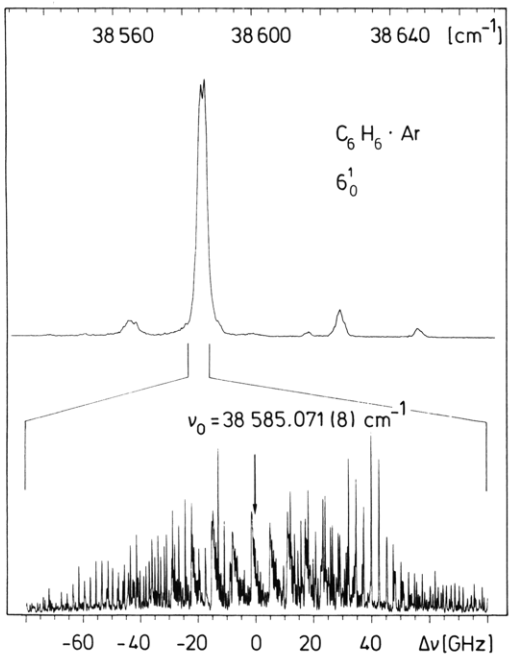


**Figure 6.** Mass-selected resonance-enhanced two-photon ionization spectra of the $6_0^1$ band of $C_6H_6$·Ar under different resolution: (upper trace) low-resolution measurement; (lower trace) rotationally resolved spectrum recorded with the experimental setup shown in Figure 5.

by only 21 $cm^{-1}$ to longer wavelength relative to the corresponding band in pure benzene.[46,47] This red shift denotes that the complex is more strongly bound in the $S_1$ state than in its electronic ground state. The upper trace in Figure 6 represents the spectrum of the $6_0^1$ band in $C_6H_6$·Ar and neighboring weak bands when measured under a spectral resolution of 0.4 $cm^{-1}$. This resolution permits the separation of the different vibronic bands. However no rotational structure is observed. A similar spectrum of the complex of benzene was first obtained by Fung et al.[46] and Menapace and Bernstein.[5] In the lower trace the same band is presented with a resolution of 120 MHz achieved in our previous work for $C_6H_6$·Ar.[42] It displays a rich fine structure of the vibronic band that is the rotational structure of a prolate symmetric top with most of the rotational lines resolved. The well-resolved strong lines at the low- and high-energy side of the spectrum are assigned to the P and R branch, respectively. The seven strong features in the center of the band are subbranches of the Q branch with partly overlapping rotational lines.

For a precise determination of the rotational constants, a two-stage computer fit to the line positions in the spectrum was performed according to a symmetric top energy formula. In the first step, the ground state constant $B_0''$ is evaluated by combination differences, i.e. frequency differences of transitions starting at different ground states but leading to the same excited state. In a second step the excited state rotational constants are fitted to about 200 unblended rotational lines. The standard deviation of the fit is 29.6 MHz which is less than a quarter of the spectral line width. The quality of the fit is demonstrated in Figure 7 for $C_6H_6$·Ar. The upper trace gives the experimental spectrum; the lower inverted scale shows the calculated spectrum with the rotational constants for the $S_0$ ground state of $A_0'' = 0.094\,880\,9$ $cm^{-1}$, $B_0'' = 0.039\,402\,576(4)$ and the $S_1,6^1$ state of $A_0' = 0.090\,866(3)$, $B_0' = 0.040\,090(2)$, and the Coriolis coupling constant of $\xi_{eff}' = -0.586\,9(9)$. A stick spectrum was calculated from the rotational constants resulting from the fit procedure described above. In the inset the central part of the band, i.e. the Q branch, is displayed on an

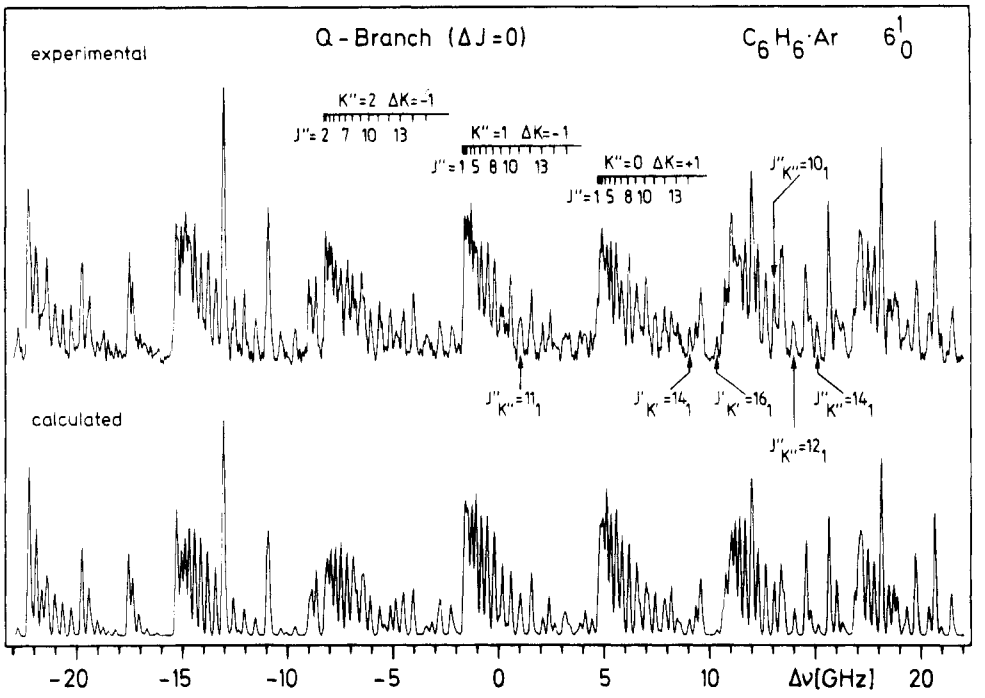


**Figure 7.** Central part (Q branch) of the $6_0^1$ band of $C_6H_6$·Ar: (upper trace) experimental spectrum; (lower trace) spectrum calculated from the rotational constants obtained from the analysis of the experimental spectrum. Several rovibronic lines with either $K'' = 1$ or $K' = 1$ and a high $J$ are marked by arrows. These lines should display a splitting if the complex structure deviates from a symmetric top.

**Table 2. Experimental Values for Different Structural and Energetic Parameters for $C_6H_6$·Ar, $C_6H_6$·$^{84}$Kr, and $C_6H_6$·$Ar_2$ Complexes**[a]

| | $C_6H_6$·Ar | | $C_6H_6$·$^{84}$Kr | | $C_6H_6$·$Ar_2$ (1\|1) |
|---|---|---|---|---|---|
| | our work | theoretical | our work | theoretical | (our work) |
| $D_0$, cm$^{-1}$ | <340[b] | 380[i]<br>393[j] | <402[b] | 450[i]<br>460[j] | |
| $E_0$, cm$^{-1}$ | <512[b] | 624[i] | <635[b] | 758[j] | |
| IE, cm$^{-1}$ | 74383 ± 2[b] | | 74322 ± 2[b] | | 74221 ± 2[d] |
| $\langle r \rangle$, Å ($S_0$) | 3.581[e] | 3.53[i]<br>3.45[j,k] | 3.674[e] | 3.71[i]<br>3.50,[j]<br>3.58[k] | 3.577[h] |
| $\langle r \rangle$, Å ($S_1$) | 3.521[e] | 3.44[l] | 3.605[e] | 3.56[k] | 3.517[h] |
| $s^1_+$, cm$^{-1}$ ($S_1$) | 40.10[f] | 44.3[i]($S_0$)<br>42[j]($S_0$) | 37.38[g] | 38.1[i]($S_0$)<br>37[j]($S_0$) | 35.8[h] |
| $s^1$, cm$^{-1}$ ($\tilde{X}$) | 48[c] | | 46[d] | | |

[a] For comparison recent theoretical results from ab initio and force field calculations are included. $D_0$,$E_0$, Dissociation energy of the neutral and ionic complex, respectively; IE, ionization energy; $\langle r \rangle$, averaged benzene–noble gas van der Waals distance, $s^1$, frequency of the van der Waals stretching mode. [b] References 12 and 70. [c] Reference 70. [d] This work. [e] Reference 48. [f] Reference 44. [g] Reference 74. [h] Reference 57. [i] Reference 51. [j] References 75 and 76. [k] Reference 77.

extended scale. We find agreement in almost every detail of the band. In particular the absence of an asymmetry splitting of the indicated lines with high $J$ and low $K$ quantum number points to a very accurate symmetric top structure of the complex.

Rotationally resolved vibronic spectra have been measured with sub-Doppler resolution for other benzene–noble gas dimers and several of their natural isotopes.[48]

**Structure.** To be a symmetric top, the Ar atom of the $C_6H_6$·Ar complex has to be located above the benzene ring on the $C_6$ rotational axis. From the vibrationally averaged rotational constants $B_0''$ and $B_v'$, accurate values for the average bond distance $\langle r_{Ar} \rangle$ in the $S_0$ and the $S_1$ state are calculated. We find a *decrease* of the van der Waals distance from 3.58 Å in the $S_0$ state to 3.52 Å in the electronically excited $S_1$ state. This can be explained by a higher polarizability of benzene in the $S_1$ state causing a stronger attractive force. In addition, the ring size of benzene increases after electronic excitation, so that the Ar atom can come closer to the benzene ring. The results for the band shift and the van der Waals bond lengths for the investigated $C_6H_6$·X (X = Ne, Ar, Kr, Xe) dimers are listed in Table 2. The moderate increase in van der Waals bond distance is caused by the increase in atomic radius with increasing mass number down the row of noble gases. This effect is partially compensated by the strong increase in polarizability and hence attractive interaction from Ne to Xe. The increase of the red shift depends linearly on the rare gas polarizability which is in line with theoretical predictions,[49] neglecting the differences of the ionization energies and the van der Waals distance of the different complexes.

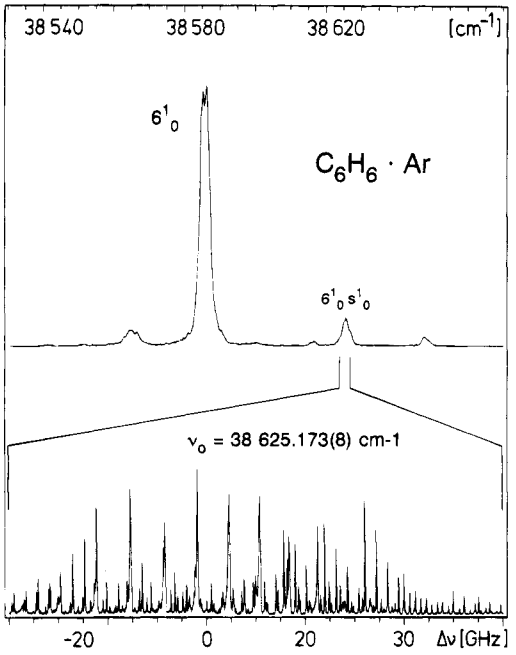


**Figure 8.** (Upper trace) low-resolution spectrum of the $6_0^1$ band of the $C_6H_6$·Ar complex and several smaller van der Waals vibronic bands and (lower trace) the rotationally resolved UV spectrum of the van der Waals band assigned as the $6_0^1s_0^1$ band (s denotes stretching vibration).

Equilibrium van der Waals distances in $C_6H_6$·X complexes have been calculated recently by ab initio methods.[50-52] They are reported in another contribution to this volume[53] and are in reasonable agreement with the experimental average values.

**van der Waals Vibrations of the Neutral Dimer.** In addition to the main $6_0^1$ band, additional weaker peaks on its blue side are seen in the vibrationally resolved spectrum in the upper trace of Figure 8 (see also Figure 6). Without additional information an assignment of these peaks in the low-resolution spectrum by intensity arguments alone is difficult and failure prone. Rotational structure can provide the necessary information. Recently we succeeded in measuring rotationally resolved spectra of all additional weak bands on the blue side of the $6_0^1$ band in $C_6H_6$·Ar, $C_6D_6$·Ar, and $C_6H_6$·Kr. In the lower trace the rotationally resolved spectrum of one of the additional bands in $C_6H_6$·Ar is represented.[45] The rotational structure of this band is similar to that of the main band shown in Figure 6. However, the slightly changed rotational constants lead to a compression of the blue-shaded Q subbranches of the $6_0^1$ band and thus to the appearance of sharp peaks in the center of the vibronic van der Waals band. From this it is clear that the additionally excited van der Waals vibration is totally symmetric and thus the stretching vibration. The frequency of the first quantum of the stretching vibration is 40.1 $cm^{-1}$. This value is in good agreement with recent theoretical results.[51,54,55] On the other hand there is still disagreement and an uncertainty in the assignment of the other van der Waals bands. This is surprising since this is the simplest possible benzene molecule containing van der Waals complex. Therefore even more difficulties are expected for molecule–molecule complexes with more van der Waals modes.

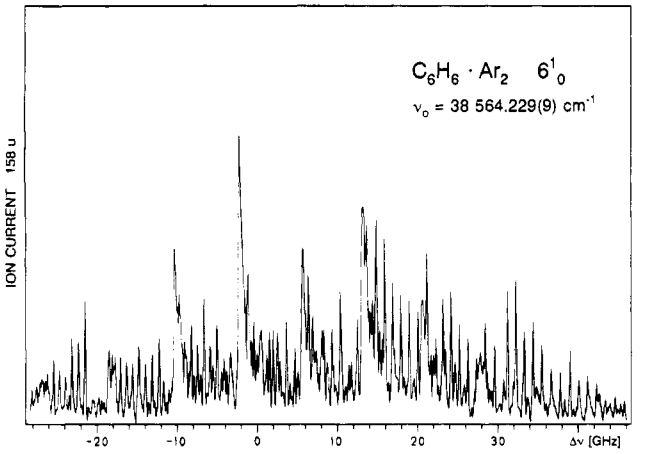


**Figure 9.** Mass-selected resonance-enhanced two-photon ionization spectrum of the $6_0^1$ band of the $C_6H_6$·$Ar_2$ complex under rotational resolution.

### *1.3. Benzene–Noble Gas Trimers*

After the structure of the $C_6H_6$·Ar complex has been explored a natural question concerns the preferred position of attachment of a further noble gas atom. Here the problem arises that the inertial moments become larger and consequently the rotational lines in the spectrum denser, making their resolution more difficult particularly for clusters containing larger aromatic molecules (see above). Furthermore it is not clear a priori whether the additional noble gas atoms are so strongly bound that fast isomerization processes leading to broadened spectra might be excluded at the vibrational temperature achieved in the molecular beam.

Our initial experimental results show that the $C_6H_6$·$Ar_2$ complex displays a sharp rotationally resolved spectrum of the vibronic band shifted 41.8 $cm^{-1}$ to the red of the bare benzene transition.[56] In Figure 9 a recent result for the $C_6H_6$·$Ar_2$ complex is given. The spectrum has been measured integrating the ion current at 158 u, i.e. the mass of $C_6H_6$·$Ar_2$. The shape of the spectrum is similar to the one shown in Figures 6 and 8 with many individual rotational lines resolved. As found for the $C_6H_6$·$Ar_2$ complex the spectrum in Figure 9 is a symmetric top spectrum. The structure of the complex deduced from the spectrum is illustrated in Figure 10. Both Ar atoms lie on the $C_6$ axis on either side of the benzene plane each at a distance of 3.58 Å ((1|1) structure). This bond distance agrees exactly with that in $C_6H_6$·Ar (see Table 2). From this we conclude that the interaction between the two noble gas atoms is effectively shielded by the aromatic ring and three-body interaction is not of importance in this configuration. From the sharpness of the rotational lines it is clear that there are no dynamic processes faster than nanoseconds and the complex displays a rigid structure. Sharp lines have been also observed for the $6_0^1s_0^1$ band of the $C_6H_6$·$Ar_2$ complex with one excited quantum of the stretching vibration in the final state.[57] This leads to the same conclusion that isomerization and dissociation processes on the subnanosecond time scale are absent in this higher excited state.

Here we must ask whether the (1|1) structure (see Figure 10) is the only structure of the $C_6H_6$·$Ar_2$

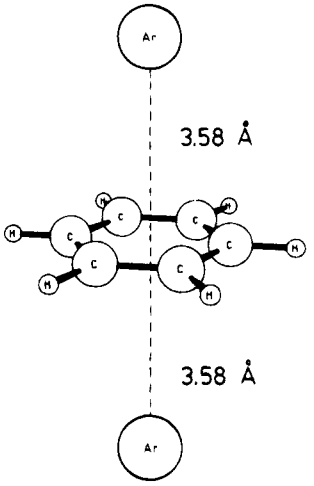


**Figure 10.** Experimentally determined structure of the $C_6H_6$·$Ar_2$ complex.

complex existing in the molecular beam. In fact, recent experiments with lower (vibrational) resolution point to the existence of an additional structural isomer with both Ar atoms on the same side of the benzene ring, (2|0).[58] This has been concluded from the different shift of the ionization energy, from the vibronic red shift in the $S_1 \leftarrow S_0$ spectrum of both isomers,[58], and from a low-resolution rotational contour analysis.[59] In a recent theoretical work,[60] it was proposed that the (2|0) isomer is becoming nonrigid above 5 K, i.e. at temperatures smaller than usually obtained in molecular beams. In contrast, the (1|1) isomer should be rigid up to 50 K. It is hardly possible to check these predictions by low-resolution spectroscopy with vibrational resolution in an unambiguous way. However, through rotationally resolved spectroscopy clear statements concerning the structure and the rigidity of the investigated complexes can be made. The sharp spectrum in Figure 9 can only originate from a complex that is stable on the nanosecond time scale. Any picosecond isomerization processes would lead to a broadening of the rotational lines. This result is in line with the theoretical predictions of ref 60.

Recently, similar results were obtained for carbazole–$Ar_2$ from high-resolution spectroscopy.[61] Like in benzene the dominating structure of carbazole·$Ar_2$ is the (1|1) structure with one Ar on each side of the carbazole plane. The other isomer (2|0) proposed in the work of Leutwyler and co-workers[62] has not yet been identified.

## 2. Production and Decay of Vibrational State-Selected Complex Ions

### 2.1. Introductory Remarks

A common characteristic of the clusters studied in section II is that they undergo strong structural changes after the ionization process. For example, in the benzene dimer, the T-shape structure of the neutral complex changes to a sandwich structure in the ion. As a consequence the vertical ionization process leads to the excitation of many intermolecular modes in the ion and the adiabatic ionization transition is weak. Some of the van der Waals modes have low frequencies and produce a smoothly increasing ionization efficiency curve with densely packed ion states rather than a steplike behavior of the ion current with each new channel separated from the preceding one. For this reason there is little chance to selectively excite defined vibrational states in these dimer ions.

In this section we focus our attention to aromatic molecule–noble gas complexes with no more than three van der Waals modes and no strong structural changes during the ionization process. We will demonstrate that in these cases the newly developed technique of delayed pulsed field threshold ionization leads to the production of vibrational state-selected complex ions.

### 2.2. Mass-Analyzed Pulsed Field Threshold Ionization (MATI)

Mass-analyzed delayed pulsed field ionization is a powerful technique when combined with narrow bandwidth laser excitation. It allows one to separate molecules in a narrow energy range close to the ionization threshold from simultaneously excited molecules in lower lying Rydberg states and from non-energy-selected ions produced by direct ionization above a lower ionization threshold. This is possible due to the strongly increasing lifetime of the Rydberg states approaching the ionization threshold. The lifetime lengthens due to an increase of the radiative and the nonradiative lifetime, both increasing with $n^3$, where $n$ is the principal quantum number. For states with $n > 100$ in many molecules this lifetime exceeds several microseconds. Thus delay times in the microsecond range can be used to field ionize the molecules in the Rydberg states. During this long delay time, the promptly produced undesired non-energy-selected ions can be spatially separated from the still neutral molecules in Rydberg states simply by applying a weak field not only sufficient to field ionize all of the latter but also to decelerate the ions.

Recently, delayed pulsed field ionization has been used to measure electrons with nearly zero kinetic energy (ZEKE).[63] The newly developed ZEKE technique of Reiser et al. displays a considerably increased resolution in photoelectron spectroscopy of the electronic ground state ions.[63–65] Recently, Zhu and Johnson presented a method to combine pulsed field ionization with ion detection.[66] In their technique they separated the threshold ions from ions below this threshold that are responsible for the background in photoionization efficiency spectra by a special technique. This includes three different acceleration regions and a time-of-flight analysis in the mass spectrometer. A similar method was presented by Jouvet et al.[67] In our recent work we introduced another versatile, easily applicable method for separation of both ion species. It is based on the energy selection in the reflecting field of a linear reflection mass spectrometer and provides high mass resolution which is particularly important for cluster investigations.[8,19]

While the ZEKE technique has provided a sub $cm^{-1}$ resolution[68] in the ion spectra the detection of threshold ions with its mass selectively (MATI) is important for the investigation of photochemical processes, e.g.

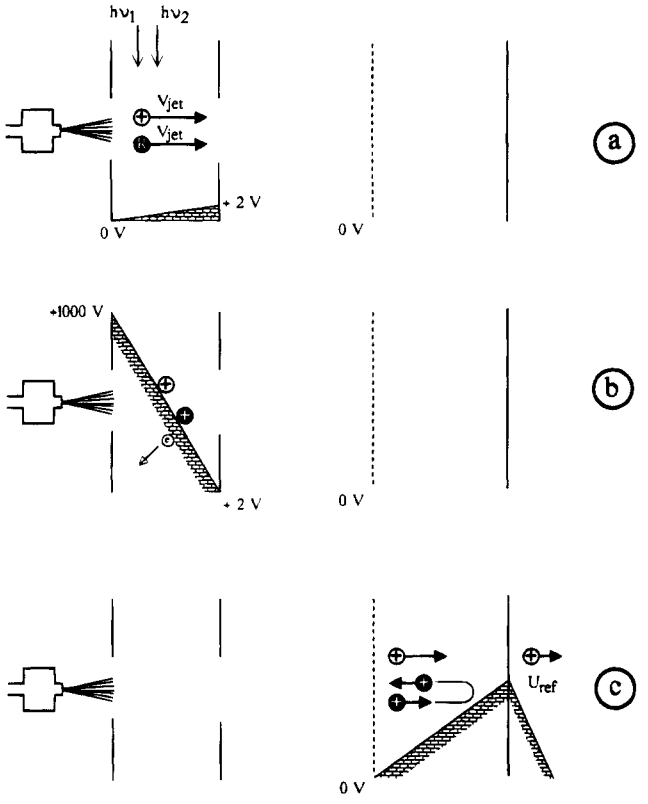


**Figure 11.** Principle of mass-selected pulsed field ionization in a reflectron time-of-flight mass spectrometer. (a, $t = 0$) Molecules are excited by resonance enhanced two-color two-photon excitation. A weak deceleration field leads to the separation of instantaneously ionized molecules (+) and the neutral Rydberg molecules (R). (b, $t \approx 5$ $\mu$s) A strong electric field is applied. It ionizes the still-existing Rydberg molecules and accelerates all ions. The directly ionized molecules are now separated from the newly produced ions and accelerated by a higher potential difference. (c, $t \approx 25$ $\mu$s) Due to their larger kinetic energy they penetrate through the reflector, whereas the ions produced by pulsed field ionization are reflected and monitored separately.

the dissociation of excited state-selected molecular and cluster ions.[8,19]

The principle of our method to separate the ions produced by pulsed field ionization (PFI) from directly ionized molecules is shown in Figure 11. The molecules enter the mass spectrometer with the velocity $v_{jet}$ of the molecular beam, which depends on the noble gas used (He or Ar). At this time ($t = 0$) a weak electric field of $E_1 \approx -0.2$ to $-0.6$ V/cm is present (Figure 11a). Its direction is chosen so that the ions instantaneously produced by the laser pulse are decelerated. In the present experiment the pulsed acceleration voltage is delayed by several microseconds after the exciting laser pulse. This is the main difference between the conventional mass spectrometric operation of the reflectron and the technique described here.

After the delay of 3−100 $\mu$s the highly excited neutral molecules in long-lived Rydberg states and the ions originally produced at the same place are spatially separated by about 1 mm in the case of 5 $\mu$s delay (Figure 11b). At this time a pulsed positive

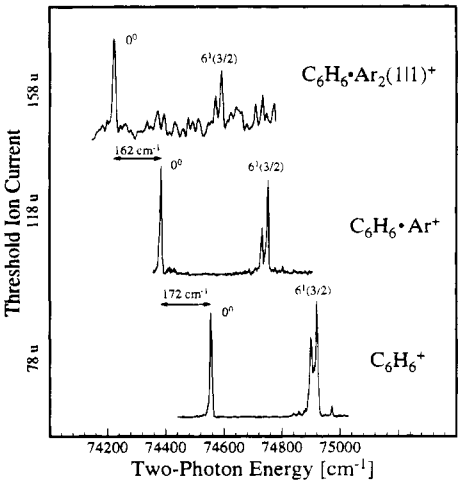


**Figure 12.** Vibrational spectra of the ionic ground state of the bare benzene cation $C_6H_6^+$ (bottom), $(C_6H_6{\cdot}Ar)^+$ cation (middle), and $(C_6H_6{\cdot}Ar_2)^+$ cation (top). Note the red shift of the adiabatic IE with increasing cluster size.

voltage of 1000 V is applied to the repeller plate. This leads to an electric field of +333 V/cm, causing the field ionization of the still existing long-lived Rydberg states and the rapid acceleration of all ions. Due to the spatial separation the instantaneously produced ions are accelerated by a higher potential difference than the ions produced by delayed PFI. For a typical spatial separation of 1 mm, this energy differences is about 33 eV. It is sufficient to separate both species within the reflector of the mass spectrometer. The reflecting voltage $U_{ref}$ is chosen so that only PFI ions are reflected while the instantaneously produced ions penetrate through the reflector (Figure 11c). In this way the PFI ions are detected after reflection and passing the second drift region.

### 2.3. Results

**$(C_6H_6{\cdot}Ar)^+$ and $(C_6H_6{\cdot}Kr)^+$ Vibrational Spectra.** Figure 12 shows the threshold ionization spectra of $C_6H_6^+$, $(C_6H_6{\cdot}Ar)^+$, and $(C_6H_6{\cdot}Ar_2)^+$ after two-photon ionization via the $6^1$ intermediate state. The left peak in each spectrum represents the $0_+^0$ vibrationless ionic ground state the double peak at higher excess energy corresponds to the $6_+^1(3|2)$ state. The $0^0$ transition $(C_6H_6{\cdot}Ar)^+$ is red shifted by 172 cm$^{-1}$ relative to that in benzene due to the stronger bonding of the $(C_6H_6{\cdot}Ar)^+$ cation compared to the neutral ground state complex. It represents the red shift of the adiabatic ionization energy after complexation. The ionization energy (IE) of $C_6H_6{\cdot}Ar$ is found to be 74383 ± 2 cm$^{-1}$ in good agreement with ZEKE results.[69] Similarly the attachment of a second argon atom leads to an additional red shift of the adiabatic IE of 162 cm$^{-1}$. The red shift of the IE represents an accurate value for the differences of the van der Waals potential depth in the $S_0$ state and the $\tilde{X}$, $^2E_{1g}$ ionic ground state. The situation is similar to the 21 cm$^{-1}$ red shift of the $6_0^1$ transition in $C_6H_6{\cdot}Ar$, indicating that the van der Waals potential in the $S_1$ state is deeper by 21 cm$^{-1}$ than in the $S_0$ ground state. In both cases *differences* in potential depth can be given with high accuracy.

Figure 13 shows the threshold spectrum of $(C_6H_6{\cdot}Ar)^+$ up to an excess energy above the IE of

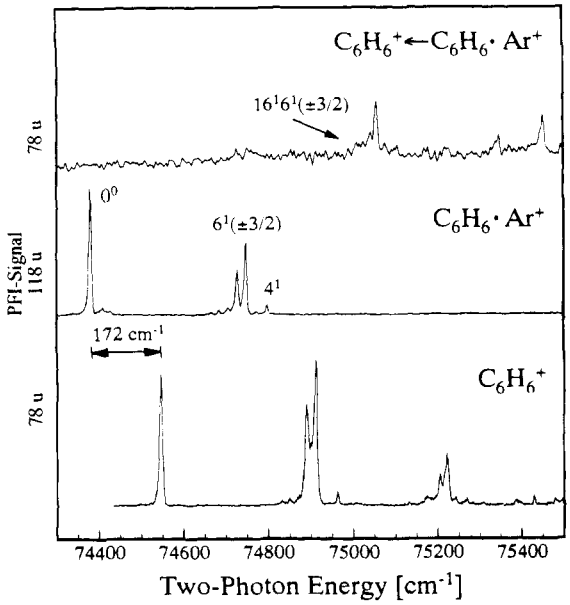


**Figure 13.** Three threshold ion spectra after two-photon ionization obtained for a molecular beam with benzene seeded in Ar under high pressure. The bottom spectrum shows the vibrational spectrum of the benzene cation measured at mass 78 u for a photon energy $h\nu_1$ in resonance with the $6^1$ state of neutral $C_6H_6$. The middle spectrum shows the vibrational spectrum of the $(C_6H_6{\cdot}Ar)^+$ cation measured at mass 118 u for a photon energy $h\nu_1$ in resonance with the $6^1$ state of the neutral $C_6H_6{\cdot}Ar$ dimer. The energy of the $0^0$ state in the $(C_6H_6{\cdot}Ar)^+$ cation is lower by 172 cm$^{-1}$ than in bare benzene. The top spectrum shows the threshold ion signal at the benzene mass 78 u for the excitation conditions of the middle spectrum with $h\nu_1$ in resonance with the $6^1$ state of the neutral $C_6H_6{\cdot}Ar$ dimer. Note that the vibrational peaks at higher energy disappear in the middle spectrum but appear in the top spectrum. For explanation, see text.

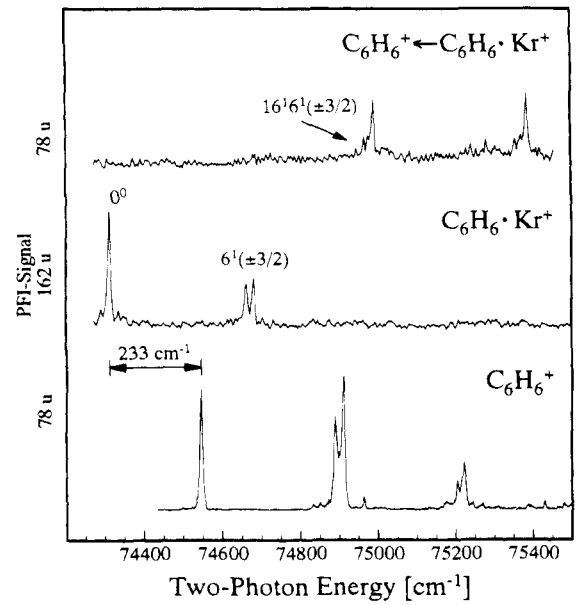


**Figure 14.** Three threshold ion spectra after two-photon ionization obtained for a molecular beam with benzene seeded in Kr under high pressure. The bottom spectrum shows the vibrational spectrum of the benzene cation measured at mass 78 u for a photon energy $h\nu_1$ in resonance with the $6^1$ state of neutral benzene. The middle spectrum shows the vibrational spectrum of the $(C_6H_6{\cdot}Kr)^+$ cation measured at mass 162 u for a photon energy $h\nu_1$ in resonance with the $6^1$ state of the neutral $C_6H_6{\cdot}Kr$ dimer. The energy of the $0^0$ state in the $(C_6H_6{\cdot}Kr)^+$ cation is lower by 233 cm$^{-1}$ than in bare benzene. The top spectrum shows the threshold ion signal at the benzene mass 78 u for the excitation conditions of the middle spectrum with $h\nu_1$ in resonance with the $6^1$ state of the neutral benzene–Kr dimer. Like in Figure 13 the vibrational peaks at higher energy disappear in the middle spectrum but appear in the top spectrum. For explanation, see text.

about 1000 cm$^{-1}$ (middle trace) compared to the $C_6H_6^+$ spectrum (bottom). The striking result in Figure 13 is the absence of any vibrational structure above the $4^1_+$ band in $(C_6H_6{\cdot}Ar)^+$. From this we conclude that photodissociation of the dimer ion has led to the disappearance of the $16^16^1_+(3|2)$ and higher peaks. The upper trace in Figure 13 confirms this conclusion. Here the signal at the daughter ($C_6H_6$) ion mass is monitored for the same excitation conditions. We clearly recognize that the lowest peak present is the $16^16^1_+(3|2)$ band which on the other hand is the first absent in the dimer ion spectrum. In addition a very weak signal is observed at the lower lying $6^1_+(3|2)$ band with an excess energy of 343 cm$^{-1}$. From this result we conclude that the $(C_6H_6{\cdot}Ar)^+$ cation dissociates on the time scale of the pulsed field delay, i.e. of less than 10 $\mu$s when 629 cm$^{-1}$ of excess energy are deposited in the dimer cation.

In Figure 14 the threshold ion spectrum of $(C_6H_6{\cdot}^{84}Kr)^+$ is shown (middle trace).[13] The mass selectivity of our technique allows one to separate the main isotopic peak of $(C_6H_6{\cdot}^{84}Kr)^+$ from the other isotopic contributions to the threshold ion current that are present in the natural isotopic mixture. The shift of the $0^0_+$ transition from that in bare benzene (lower trace) is 233 cm$^{-1}$, i.e. larger than in $(C_6H_6{\cdot}Ar)^+$. This is due to the stronger bonding caused by the larger polarizability of Kr. In Figure 15 the threshold ion spectrum in the vicinity of the adiabatic ionization energy of the $C_6H_6{\cdot}^{84}Kr$ complex is shown in more detail. In the lower trace the $6^1$ state without an additional van der Waals mode was taken as the intermediate state. No pronounced additional van der Waals peaks are seen on the blue side of the $0^0_+$ origin. This demonstrates that Franck–Condon factors favor the conservation of the vibrational state

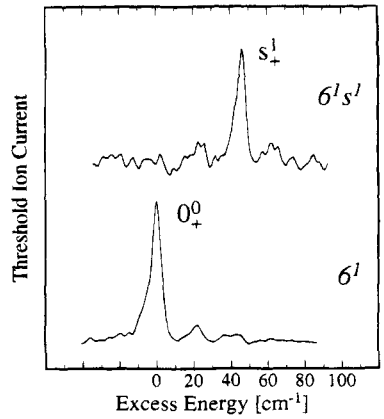


**Figure 15.** Two threshold ion spectra in the region of the $0^0_+$ band of the $(C_6H_6{\cdot}^{84}Kr)^+$ dimer cation. (Lower trace) Intermediate state is the $6^1$ state in the $S_1$ state of the neutral $C_6H_6{\cdot}Kr$ dimer. Van der Waals vibrations are not excited. (Upper trace) Intermediate state is the $6^1s^1$ state in the $S_1$ state neutral $C_6H_6{\cdot}Kr$ dimer (s indicates the stretching vibration).

in the second absorption step to the ionic state. This is a reasonable result for the heterogeneous benzene–noble gas van der Waals dimers since there are no strong contributions to the binding in the cluster ion from charge transfer resonance interaction and only slight structural changes after ionization.

No Jahn–Teller splitting of the $0_+^0$ level with $j_k = {}^1/_2$ is expected either for $(C_6H_6)^+$ or for $(C_6H_6{\cdot}^{84}Kr)^+$ since the $^2E_{1g}$ electronic symmetry of the ionic ground state $(C_6H_6)^+$ ($^2E_1$ in $(C_6H_6{\cdot}^{84}Kr)^+$) cannot be removed by the quadratic Jahn–Teller effect. This is in line with the experimental finding that a single peak appears. From the small quadratic Jahn–Teller coupling constant of benzene found in our recent work,[70] we concluded that the three potential minima resulting from the quadratic Jahn–Teller effect are shallow in $(C_6H_6)^+$ and separated by a very low barrier. The vibrational zero-point level will be above the barrier and on the average the 6-fold symmetry axis is preserved. Thus we expect that in $(C_6H_6{\cdot}^{84}Kr)^+$ the $^{84}Kr$ atom is located on the 6-fold symmetry axis just as in the neutral $C_6H_6{\cdot}^{84}Kr$.[48] Hence the discussion of the $0_+^0$ band and its totally symmetric van der Waals progressions is straight forward and no asymmetrically distorted configuration of the $(C_6H_6{\cdot}^{84}Kr)^+$ complex has to be considered. A different situation may occur if the degenerate bending van der Waals vibration were excited. It has to be checked whether this mode is Jahn–Teller active. This could lead to a splitting of the transition and a lifting of its degeneracy.

With the above-mentioned propensity rule in mind we can now interpret the upper spectrum of Figure 15. Here the $6^1s^1$ state with one additional quantum of the stretching vibration is excited as the intermediate state as indicated. The frequency of the $s^1$ van der Waals vibration in the intermediate state is known from the rotationally resolved spectra discussed in section III.1 (see Table 2). We expect that the propensity rule discussed above leads preferentially to the excitation of one quantum of the stretching vibration in the $0_+^0$ state. We assign the strong peak at 46 $cm^{-1}$ to the $s_+^1$ vibration. The somewhat larger frequency of 46 $cm^{-1}$ of the stretching vibration in the $(C_6H_6{\cdot}^{84}Kr)^+$ cation (compared to 37.4 $cm^{-1}$ in the $S_1$ state) is reasonable when we take into account that the ionic complex is more strongly bound by 199.6 $cm^{-1}$ than the neutral complex in the $S_1$ state. Higher states of the van der Waals vibrations can be excited using higher vibrational van der Waals bands (see Figure 8) as intermediate states for the resonance-enhanced ionization process. This was demonstrated for the $(C_6H_6{\cdot}Ar)^+$ ion complex in our recent work.[70]

### 2.4. Discussion

**Dissociation Mechanism.** First we briefly discuss an alternative mechanism that could lead to the breakdown of the signal on the parent ion mass above 418 $cm^{-1}$ and the appearance of signal at the daughter ion mass. In principle, the appearance of the $(C_6H_6{\cdot}Ar)^+$ spectrum at the $C_6H_6^+$ mass channel could be due to a preceding transfer of the Rydberg electron from the $C_6H_6{\cdot}Ar$ to a neighboring ionized $C_6H_6^+$ molecule, where it could be bound again as a Rydberg electron. Then after field ionization one would detect a benzene cation with, however, the spectral characteristic and IE's of the initially excited $(C_6H_6{\cdot}Ar)^+$ dimer. For this electron transfer a sufficiently high probability for a Rydberg–ion collision would be necessary. An estimate of the molecular density within the jet shows that similar to previous findings,[71] the neutral molecule density and also the ion density is too large to be able to exclude an electron-transfer process during the microsecond interaction time of Rydberg molecules and promptly produced ions. It is, however, hard to explain why an electron-transfer process should strongly depend on the vibrational energy within the core of the Rydberg excited complex, as is found experimentally (see Figures 13 and 14). This internal energy dependence clearly points to a dissociation process of the $(C_6H_6{\cdot}Ar)^+$ and $(C_6H_6{\cdot}Kr)^+$ complex as discussed above.

From mass spectrometric arguments discussed in our previous publications,[13,14] it is clear that dissociation of the core occurs before the electron is pulsed out of the Rydberg state by the pulsed field. In other words, the Ar atom is traveling beyond the Rydberg orbit without ionizing the molecule.

**Dissociation Energies.** As shown in section 2.3 a clearly detected dissociation signal results from the $16^16^1(3|2)$ level in $(C_6H_6{\cdot}Ar)^+$ and $(C_6H_6{\cdot}Kr)^+$ at an excess energy of 629 and 635 $cm^{-1}$, respectively. Thus we find upper limits for the dissociation energy $E_0 < 629$ $cm^{-1}$ for $(C_6H_6{\cdot}Ar)^+$ and $E_0 \leq 635$ $cm^{-1}$ for $(C_6H_6{\cdot}^{84}Kr)^+$ which are very similar. However, we have to bear in mind that the real value for the dissociation energy $E_0$ of $(C_6H_6{\cdot}Ar)^+$ is considerably smaller than the real value of $E_0$ for $(C_6H_6{\cdot}Kr)^+$ because the polarizability of Kr (2.49 $Å^3$) is larger than that of Ar (1.64 $Å^3$). It is not possible to check this experimentally since there is no vibrational state of $(C_6H_6{\cdot}Ar)^+$ between the $4^1$ and the $16^16^1(3|2)$ level, which could be closer to the true dissociation energy. Furthermore, it is difficult to find lower limits for the dissociation energy since we cannot exclude a weak metastable signal produced by slow dissociation in the drift region of the mass spectrometer. With the very accurate shifts $\Delta IE$ of the IE's in $C_6H_6{\cdot}Ar$ and $C_6H_6{\cdot}Kr$ and the relation $D_0 = E_0 - \Delta IE$ we find the following upper limits for the dissociation energy $D_0$ of the neutral complexes $C_6H_6{\cdot}Ar$ (BAr) and $C_6H_6{\cdot}Kr$ (BKr):

$$D_0(BAr) \leq 457 \text{ cm}^{-1}$$

$$D_0(BKr) < 402 \text{ cm}^{-1}$$

Since the dissociation energy of $C_6H_6{\cdot}Ar$ cannot be larger than that of $C_6H_6{\cdot}Kr$ we have to replace the upper limit of $D_0(BAr)$ by the upper limit of $D_0(BKr)$:

$$D_0(BAr) < 402 \text{ cm}^{-1}$$

$$D_0(BKr) < 402 \text{ cm}^{-1}$$

With the accurate shift $\Delta IE$ of $C_6H_6{\cdot}Ar$ and $C_6H_6{\cdot}Kr$ we obtain new smaller values for the upper limits of $E_0$:

$$E_0(BAr^+) < 574 \text{ cm}^{-1}$$

$$E_0(BKr^+) < 635\ cm^{-1}$$

Again the upper limit of 574 $cm^{-1}$ of $(C_6H_6{\cdot}Ar)^+$ seems to be too high compared to the upper limit of 635 $cm^{-1}$ of $(C_6H_6{\cdot}Kr)^+$.

At this point we would like to compare the experimental results with theoretical predictions. Recent ab initio calculation of Hobza et al.[51] yielded a value for the potential depth in the neutral complex of $D_0(BKr) \approx 450\ cm^{-1}$. This result is somewhat larger than the largest possible experimental value $D_0(BKr) < 402\ cm^{-1}$. Even though the theoretical value for $D_0(BKr)$ is too high we may assume that the theoretical ratio $D_0(BKr)/D_0(BAr) \approx 0.85$ of ref 51 is realistic. Accepting the experimental value $D_0(BKr) < 402\ cm^{-1}$ we can correct the upper limit for $D_0(BAr)$ by this factor and finally obtain

$$D_0(BAr) < 340\ cm^{-1}$$

This upper limit is again somewhat smaller than the most recent theoretical value of $D_0(BAr) \approx 380\ cm^{-1}$.[51] All experimental upper limits and theoretical results from different calculations are listed in Table 2. As a general trend we find that all theoretical results are larger than the experimental upper limits.

The good agreement of the results from force field and ab initio calculations for the neutral complexes seems to support the theoretical results. However, in addition to the disagreement of experimental and theoretical dissociation energies there is another striking discrepancy between force field results and experimental values: The calculated results for the red shift of the IE's (i.e. the differences of dissociation energies of ionic and neutral complex) differ strongly from the respective experimental value both in $C_6H_6{\cdot}Ar$ (231 $cm^{-1}$ vs 172 $cm^{-1}$) and in $C_6H_6{\cdot}Kr$ (298 $cm^{-1}$ vs 233 $cm^{-1}$). There is no doubt about the experimental value. With the technique in this work it can be measured with an accuracy of a few $cm^{-1}$ (see Figures 12–14). For a more conclusive comparison with experimental results ab initio calculations for the ionic complexes would be extremely useful. Then the precisely known shift of the ionization energy could serve as a critical test of the theory.

Similarly experimental results for the *p*-difluorobenzene·Ar complex[72] point to a lower dissociation energy compared to recent ab initio calculations.[73] Pulsed field threshold ionization experiments on larger molecule–noble gas complexes are in progress. For these complexes the higher density of vibrational states should lead to even more accurate values of the dissociation energy.

## VI. Summary and Conclusion

In this work we demonstrated that newly developed spectroscopic techniques yield precise information on the structure and energetics of small van der Waals molecules. For the prototype systems of benzene with noble gases we found precise van der Waals distances from high-resolution UV spectroscopy. Rigid structures with sharp rotational lines have been detected not only for benzene–noble gas dimers but also for trimers with two Ar atoms attached to the benzene ring. Rotationally resolved spectroscopy of van der Waals vibronic bands is helpful for their assignment. The resulting van der Waals vibrational energy and the vibrationally averaged rotational constants contain information on the intermolecular potential essential for modeling of physical and chemical properties of these prototypes complexes. Energetic data are obtained in a direct way from observation of the dissociation of dimer ions produced by two-photon ionization in a time-of-flight mass spectrometer. Delayed pulse field ionization of the excited high Rydberg states of the dimers allows one to produce vibrational state-selected dimer ions and to monitor their decay as a function of the excited vibrational state. In this way information on the binding energy of neutral and ionic dimers is achieved.

In van der Waals molecules of larger components, more than three intermolecular vibrations exist. At present the application of the high-resolution and the pulsed field ionization technique does not lead to reasonable results probably because of the low-frequency van der Waals modes congesting the $S_1 \leftarrow S_0$ spectrum as well as the ion spectrum. Here the breakdown technique observing metastable daughter ion efficiency curves is applicable, yielding energetic information on the dissociation energy of neutral and ionic complexes. The strong increase of the binding energy in ionic dimers consisting of molecules with delocalized $\pi$ electrons and similar ionization energy point to a strong contribution from charge-transfer resonance interaction to the intermolecular bonding.

It is the purpose of future work to apply the experimental methods described in this work to van der Waals molecules consisting of even larger components. Precise structural and energetic information on van der Waals molecules with four or more weakly bound noble gases attached to an aromatic molecule components might be accessible if lower vibrational temperatures can be achieved in the molecular beams. This would lead to a rigidity of the larger complexes allowing e.g. the application of high-resolution techniques.

*Acknowledgments.* The authors thank the Deutsche Forschungsgemeinschaft and the Fonds der chemischen Industrie for financial support of this work. They thank B. Ernstberger and Th. Grebner for valuable discussions.

## References

(1) Beswick, J. A.; Jortner, J. *Adv. Chem. Phys.* **1981**, *47* (Part 1), 263.
(2) Jortner, J.; Scharf, D.; Landman, U. In *Elemental and Molecular Clusters*; Benedek, de G., Martin, T. P., Pacchioni, G., Eds.; Springer: Berlin, 1988.
(3) Leutwyler, S.; Bösiger, J. *Chem. Rev.* **1990**, *90*, 489.
(4) Castleman, A. W., Jr.; Keesee, R. G. *Annu. Rev. Phys. Chem.* **1986**, *37*, 525.
(5) Menapace, J. A.; Bernstein, E. R. *J. Phys. Chem.* **1987**, *91*, 2533.
(6) Wanna, J.; Menapace, J. A.; Bernstein, E. R. *J. Chem. Phys.* **1986**, *85*, 1795.
(7) Garret, A. W.; Pribble, R. N.; Gotch, A. J.; Zwier, T. S. Resonant Two-Photon Ionization Studies of $C_6H_6$-$X_n$ Clusters. In *Advances in Multiphoton Processes and Spectroscopy*; Villaeys, A. A., Fujimura, Y., Eds.; World Scientific: Singapore, 1994; Vol. 9.
(8) Kiermeier, A.; Ernstberger, B.; Neusser, H. J.; Schlag, E. W. *J. Phys. Chem.* **1988**, *92*, 3785.
(9) Ernstberger, B.; Krause, H.; Kiermeier, A.; Neusser, H. J. *J. Chem. Phys.* **1990**, *92*, 5285.
(10) Ernstberger, B.; Krause, H.; Neusser, H. J. *Z. Phys. D* **1991**, *20*, 189.
(11) Krause, H.; Ernstberger, B.; Neusser, H. J. *Chem. Phys. Lett.* **1991**, *184*, 411.

(12) Krause, H.; Neusser, H. J. *J. Chem. Phys.* **1992**, *97*, 5923.
(13) Krause, H.; Neusser, H. J. *J. Chem. Phys.* **1993**, *99*, 6278.
(14) Neusser, H. J.; Krause, H. *Int. J. Mass Spectrom. Ion Proc.* **1994**, *131*, 211.
(15) Lifshitz, C.; Ohmichi, N. *J. Phys. Chem.* **1989**, *93*, 6329.
(16) Chupka, W. A. *J. Chem. Phys.* **1959**, *30*, 191.
(17) Chupka, W. A.; Berkowitz, J. *J. Chem. Phys.* **1967**, *47*, 2921.
(18) Nimlos, M. R.; Young, M. A.; Bernstein, E. R.; Kelley, D. F. *J. Chem. Phys.* **1989**, *91*(9), 5268.
(19) Kühlewind, H.; Neusser, H. J.; Schlag, E. W. *Int. J. Mass Spectrom. Ion Phys.* **1983**, *51*, 255.
(20) Selzle, H. L.; Neusser, H. J.; Ernstberger, B.; Krause, H.; Schlag, E. W. *J. Phys. Chem.* **1989**, *93*, 7535.
(21) Dehmer, P. M. *J. Chem. Phys.* **1982**, *76*, 1263.
(22) Rühl, E.; Brutschy, B.; Baumgärtel, H. *Chem. Phys. Lett.* **1989**, *157*, 379.
(23) Grover, J. R.; Hagenow, G.; Walters, E. A. *J. Chem. Phys.* **1992**, *97*, 628.
(24) Fung, K. H.; Henke, W. E.; Hays, T. R.; Selzle, H. L.; Schlag, E. W. *J. Phys. Chem.* **1981**, *85*, 3560.
(25) Scherzer, W.; Krätzschmar, O.; Selzle, H. L.; Schlag, E. W. *Z. Naturforsch.* **1992**, *47a*, 1248.
(26) Weast, R. C.; Astle, M. J. *Handbook of Chemistry and Physics*; CRC Press: Boca Raton, 1979.
(27) McClellan, A. L. *Tables of Experimental Dipole Moments*; Rahara Enterprises: El Cerrito, 1974.
(28) van de Waal, B. W. *Chem. Phys. Lett.* **1986**, *123*, 69.
(29) de Meijere, A.; Huisken, F. *J. Chem. Phys.* **1990**, *92*, 5826.
(30) Čársky, P.; Selzle, H. L.; Schlag, E. W. *Chem. Phys.* **1988**, *125*, 165.
(31) Hobza, P.; Selzle, H. L.; Schlag, E. W. *J. Chem. Phys.* **1990**, *93*, 5893.
(32) Badger, B.; Brocklehurst, B. *Nature* **1968**, *219*, 263.
(33) McConnell, H. M. *J. Chem. Phys.* **1961**, *35*, 508.
(34) Meot-Ner, M.; Hamlet, P.; Hunter, E. P.; Field, F. H. *J. Am. Chem. Soc.* **1978**, *100*, 5466.
(35) Hiraoka, K.; Fujimaki, S.; Aruga, K.; Yamabe, S. *J. Chem. Phys.* **1991**, *95*, 8413.
(36) Demtröder, W. *Laser Spectroscopy*, 3rd ed.; Springer: Berlin, 1988.
(37) Boesl, U.; Neusser, H. J.; Schlag, E. W. *Z. Naturforsch.* **1978**, *33a*, 1546.
(38) Boesl, U.; Neusser, H. J.; Schlag, E. W. *J. Am. Chem. Soc.* **1981**, *103*, 5058.
(39) Hopkins, J. B.; Powers, D. E.; Smalley, R. E. *J. Phys. Chem.* **1981**, *85*, 3739.
(40) Fung, K. H.; Selzle, H. L.; Schlag, E. W. *J. Phys. Chem.* **1983**, *87*, 5113.
(41) Leutwyler, S.; Even, U.; Jortner, J. *Chem. Phys. Lett.* **1982**, *86*, 439.
(42) Weber, Th.; von Bargen, A.; Riedle, E. Neusser, H. J. *J. Chem. Phys.* **1990**, *92*, 90.
(43) Riedle, E.; Moder, R.; Neusser, H. J. *Opt. Commun.* **1982**, *43*, 388.
(44) Riedle, E.; Knittel, Th.; Weber, Th.; Neusser, H. J. *J. Chem. Phys.* **1989**, *91*, 4555.
(45) Neusser, H. J.; Sussmann, R.; Smith, A. M.; Riedle, E.; Weber, Th. *Ber. Bunsen-Ges. Phys. Chem.* **1992**, *96*, 1252.
(46) Fung, K. H.; Selzle, H. L.; Schlag, E. W. *Z. Naturforsch.* **1981**, *36a*, 1338.
(47) Gonohe, N.; Suzuki, N.; Abe, H.; Mikami, N.; Ito, M. *Chem. Phys. Lett.* **1983**, *94*, 549.
(48) Weber, Th.; Riedle, E.; Neusser, H. J.; Schlag, E. W. *Chem. Phys. Lett.* **1991**, *183*, 77.
(49) Leutwyler, S.; Even, U.; Jortner, J. *J. Chem. Phys.* **1983**, *79*, 5769.
(50) Hobza, P.; Selzle, H. L.; Schlag, E. W. *J. Chem. Phys.* **1991**, *95*, 391.
(51) Hobza, P.; Bludsky, O.; Selzle, H. L.; Schlag, E. W. *J. Chem. Phys.* **1992**, *97*, 335.
(52) Brupbacher, Th.; Lüthi, H. P.; Bauder, A. *Chem. Phys. Lett.* **1992**, *195*, 482.
(53) Hobza, P.; Selzle, H. L.; Schlag, E. W. *Chem. Rev.* **1994**, *94*, this issue.
(54) Bludsk'y, O.; Spirko, V.; Hrouda, V.; Hobza, P. *Chem. Phys. Lett.* **1992**, *196*, 410.
(55) van der Avoird, A. *J. Chem. Phys.* **1993**, *98*, 5327.
(56) Katakuse, J.; Ito, H.; Ichihara, T. *Z. Phys. D* **1991**, *20*, 101.
(57) Weber, Th.; Neusser, H. J. *J. Chem. Phys.* **1991**, *94*, 7689.
(58) Schmidt, M.; Mons, M.; Le Calvé, J. *Chem. Phys. Lett.* **1991**, *177*, 371.
(59) Schmidt, M.; Mons, M.; Le Calvé, J.; Millié, P.; Cossart-Magos, C. *Chem. Phys. Lett.* **1991**, *183*, 69.
(60) Ben-Horin, N.; Even, U.; Jortner, J. *Chem. Phys. Lett.* **1992**, *188*, 73.
(61) Sussmann, R.; Neusser, H. J. *Chem. Phys. Lett.* **1994**, *221*, 46.
(62) Leutwyler, S.; Bösiger, J. *Z. Phys. Chem.* **1987**, *154*, 31.
(63) Reiser, G.; Habenicht, W.; Müller-Dethlefs, K.; Schlag, E. W. *Chem. Phys. Lett.* **1988**, *152*, 119.
(64) Müller-Dethlefs, K.; Schlag, E. W. *Annu. Rev. Phys. Chem.* **1991**, *42*, 109.
(65) Müller-Dethlefs, K.; Dopfer, O.; Wright, T. G. *Chem. Rev.* **1994**, *94*, this issue.
(66) Zhu, L.; Johnson, P. *J. Chem. Phys.* **1991**, *94*, 5769.
(67) Jouvet, C.; Dedonder-Lardeux, C.; Martrenchard-Barra, S.; Solgadi, D. *Chem. Phys. Lett.* **1992**, *198*, 419.
(68) Sekiya, H.; Lindner, R.; Müller-Dethlefs, K. *Chem. Lett.* **1993**, 485.
(69) Chewter, L. A.; Müller-Dethlefs, K.; Schlag, E. W. *Chem. Phys. Lett.* **1987**, *135*, 219.
(70) Krause, H.; Neusser, H. J. *Chem. Phys. Lett.* **1993**, *213*, 603.
(71) Zhang, X.; Smith, J. M.; Knee, J. L. *J. Chem. Phys.* **1992**, *97*, 2843.
(72) Su, M.-C.; O, H.-K.; Parmenter, C. S. *Chem. Phys.* **1991**, *156*, 261.
(73) Hobza, P.; Selzle, H. L.; Schlag, E. W. *J. Chem. Phys.* **1993**, *99*, 2809.
(74) Riedle, E.; Sussmann, R.; Weber, Th.; Neusser, H. J. To be published.
(75) Horin, N. B.; Even, U.; Jortner, J. *J. Chem. Phys.* **1989**, *91*, 331.
(76) Leutwyler, S.; Jortner, J. *J. Phys. Chem. 91*, **1987**, 5558.
(77) Kim, H. Y.; Cole, M. W. *J. Chem. Phys.* **1989**, *90*, 6055.